



American Society of Hematology
 2021 L Street NW, Suite 900,
 Washington, DC 20036
 Phone: 202-776-0544 | Fax 202-776-0545
 editorial@hematology.org

An in vivo barcoded CRISPR-Cas9 screen identifies Ncoa4-mediated ferritinophagy as a dependence in Tet2-deficient hematopoiesis

Tracking no: BLD-2024-028033R1

Justin Loke (Dana-Farber Cancer Institute, United States) Peter Kim (Dana-Farber Cancer Institute, United States) Thuy Nguyen (Dana-Farber Cancer Institute,, United States) Meaghan Boileau (Dana Farber Cancer Institute, United States) Marie McConkey (Dana-Farber Cancer Institute, United States) Aidan Miller (Dana-Farber Cancer Institute, United States) Wesley Shin (Dana-Farber Cancer Institute, United States) Christopher Hergott (Brigham and Women's Hospital, United States) Maria Ericsson (Harvard Medical School, United States) Anja Nordstrom (Harvard Medical School, United States) Paula Montero-Llopis (Harvard Medical School, United States) Scott Armstrong (Dana-Farber Cancer Institute, United States) Joseph Mancias (Dana-Farber Cancer Institute, United States) Benjamin Ebert (Dana-Farber Cancer Institute, United States)

Abstract:

TET2 is among the most commonly mutated genes in both clonal hematopoiesis and myeloid malignancies, thus, the ability to identify selective dependencies in TET2 deficient cells has broad translational significance. Here, we identify regulators of Tet2 knockout (KO) hematopoietic stem and progenitor cell (HSPC) expansion using an in vivo CRISPR-Cas9 KO screen, in which nucleotide barcoding enabled large-scale clonal tracing of Tet2 deficient HSPCs in a physiological setting. Our screen identified candidate genes, including Ncoa4, that are selectively required for Tet2 KO clonal outgrowth compared to wild-type (WT). Ncoa4 targets ferritin for lysosomal degradation (ferritinophagy), maintaining intracellular iron homeostasis by releasing labile iron (Fe²⁺) in response to cellular demands. In Tet2-deficient HSPCs, increased mitochondrial ATP production correlates with increased cellular iron requirements, and in turn, promotes Ncoa4-dependent ferritinophagy. Restricting iron availability reduces Tet2 KO stem cell numbers, revealing a dependency in TET2-mutated myeloid neoplasms.

Conflict of interest: COI declared - see note

COI notes: B.L.E. has received research funding from Novartis and Calico. He has received consulting fees from Abbvie. He is a member of the scientific advisory board and shareholder for Neomorph Inc., Big Sur Bio, Skyhawk Therapeutics, and Exo Therapeutics. C.B.H. has received consulting fees from 48 Bio. S.A.A. has been a consultant and/or shareholder for Neomorph, C4 Therapeutics, Hyku Therapeutics, Stelexis Therapeutics and Nimbus Therapeutics. S.A.A. has received research support from Janssen and Syndax. S.A.A. is an inventor on a patent related to MENIN inhibition WO/2017/132398A1. J.D.M. is an inventor on a patent related to targeting ferritinophagy WO/2015/149006A3. J.D.M. also reports research support from Novartis and Casma Therapeutics and has consulted for Third Rock Ventures and Skyhawk Therapeutics, all unrelated to the submitted work. J.L. has received consulting fees from TScan and honoraria from Jazz pharmaceuticals. The rest of the authors declare no further conflict of interest.

Preprint server: No;

Author contributions and disclosures: J.L., P.G.K., B.L.E. designed the study and wrote the manuscript. J.L., P.G.K., T.T.P.N., M.B., M.M., A.M., W.S., C.B.H., M.E., A.N., P.M.L., performed and analyzed experiments., S.A.A., J.D.M. contributed research tools and helped design the study. All authors reviewed and edited the manuscript.

Non-author contributions and disclosures: No;

Agreement to Share Publication-Related Data and Data Sharing Statement: scRNA-seq data has been deposited at Gene Expression Omnibus (GEO) GSE289732. For any additional data inquiries, please contact the corresponding author.

Clinical trial registration information (if any):

An in vivo barcoded CRISPR-Cas9 screen identifies *Ncoa4*-mediated ferritinophagy as a dependence in *Tet2*-deficient hematopoiesis

(Characters: 126/140)

Justin Loke* (1,2), Peter G. Kim* (1), Thuy T. P. Nguyen (3), Meaghan Boileau (4), Marie McConkey (1), Aidan Miller (1), Wesley Shin (1), Christopher B. Hergott (1,5), Maria Ericsson (6), Anja Nordstrom (6), Paula Montero Llopis (7), Scott Armstrong (4), Joseph D. Mancias (3), Benjamin L. Ebert (1,8)

1 Department of Medical Oncology, Dana-Farber Cancer Institute, Boston, MA
2 University of Birmingham, Birmingham, United Kingdom
3 Department of Radiation Oncology, Dana-Farber Cancer Institute, Boston, MA
4 Department of Pediatric Oncology, Dana-Farber Cancer Institute, Boston, MA
5 Department of Pathology, Brigham and Women's Hospital, Boston, MA
6 Department of Cell Biology, Harvard Medical School, Boston, MA
7 MicRoN Core, Harvard Medical School, Boston, MA
8 Broad Institute, Cambridge, MA

Correspondence:

Benjamin L. Ebert

Dana-Farber Cancer Institute, 450 Brookline Ave, Boston, MA, 02115

e-mail: benjamin_ebert@dfci.harvard.edu

*Contributed equally to this paper.

Data sharing statement

scRNA-seq data has been deposited at Gene Expression Omnibus (GEO) GSE289732. For any additional data inquiries, please contact the corresponding author.

Abstract (144/250 words)

TET2 is among the most commonly mutated genes in both clonal hematopoiesis and myeloid malignancies, thus, the ability to identify selective dependencies in *TET2* deficient cells has broad translational significance. Here, we identify regulators of *Tet2* knockout (KO) hematopoietic stem and progenitor cell (HSPC) expansion using an *in vivo* CRISPR-Cas9 KO screen, in which nucleotide barcoding enabled large-scale clonal tracing of *Tet2* deficient HSPCs in a physiological setting. Our screen identified candidate genes, including *Ncoa4*, that are selectively required for *Tet2* KO clonal outgrowth compared to wild-type (WT). *Ncoa4* targets ferritin for lysosomal degradation (ferritinophagy), maintaining intracellular iron homeostasis by releasing labile iron (Fe²⁺) in response to cellular demands. In *Tet2*-deficient HSPCs, increased mitochondrial ATP production correlates with increased cellular iron requirements, and in turn, promotes *Ncoa4*-dependent ferritinophagy. Restricting iron availability reduces *Tet2* KO stem cell numbers, revealing a dependency in *TET2*-mutated myeloid neoplasms.

Key Points (140 characters each):

- 1) A barcoded *in vivo* CRISPR-Cas9 knockout screen identifies *Ncoa4* as a dependency in *Tet2* mutant hematopoietic stem-progenitor cells.
- 2) In *Tet2* mutant stem-progenitor cells, *Ncoa4*-mediated ferritinophagy maintains iron availability for increased mitochondrial ATP production.

Introduction

Loss-of-function mutations in *TET2* are commonly found in clonal hematopoiesis of indeterminate potential (CHIP) as well as in hematological malignancies, including myelodysplastic syndrome (MDS) and acute myeloid leukemia (AML)¹. CHIP is maintained over the lifetime of an individual², consistent with the presence of driver mutations in hematopoietic stem cells (HSCs)³. *TET2* is an iron and 2-oxoglutaric acid-dependent enzyme that catalyzes the oxidation of methyl-cytosine resulting in demethylation of the cytosine residue⁴. Conditional knockout (KO) modeling of *Tet2* in the murine hematopoietic system faithfully recapitulates clonal expansion observed in CHIP through increased hematopoietic stem cell (HSC) renewal and pre-malignancy^{5,6}.

Both CHIP and normal HSCs reside in a specialized bone marrow niche with specific nutrient availability, cellular interactions, and cytokine and chemokine exposure⁷⁻¹⁰. HSCs with CHIP mutations may re-model bone marrow microenvironments and depend on secreted factors at precise concentrations for their expansion¹¹⁻¹³. Genetic screens have the ability to identify selective dependencies in somatically mutated cells, and *in vivo* screens have the potential to access aspects of normal and neoplastic biology that exist only within the native HSC microenvironment. A central challenge of such screens is the tremendous diversity of differentiation and proliferative potential of hematopoietic stem and progenitor cells (HSPCs)¹⁴⁻¹⁸. This challenge of cellular heterogeneity in an *in vivo* CRISPR-Cas9 screen can be addressed using barcoding strategies to track simultaneously the clonal progeny of each virally transduced HSPC clone and the corresponding effect of the single guide-RNA (sgRNA) mediated genetic perturbation.

In this study, we developed an *in vivo* barcoded CRISPR-Cas9 screening methodology to identify genetic dependencies in HSPCs and applied this technique to identify novel regulators of *TET2* mutant expansion in a model of CHIP. We provide orthogonal validation using a genetic KO mouse model and pharmacological manipulation of the target pathway. Finally, we utilize both *in vivo* and *in vitro* experiments in primary mouse and human HSPCs to provide a rationale to the synthetic lethal vulnerability observed in *TET2* KO as compared to WT HSPCs.

Methods

Barcoded CRISPR-Cas9 sgRNA Library construction

Barcoded libraries were constructed by cloning UMIs into the KflI site of the CROPseq-guide-puro vector using Gibson Assembly (NEB)¹⁹. Custom library targeting all transcription and chromatin factors were generated based on previously established lists^{20,21}. Single guide RNAs were picked using the GUIDES algorithm²². Lentiviral particles were generated via transfection of HEK293T cells using FuGENE (Promega). Viral constructs were co-transfected with pMD2.G (plasmid 12259; Addgene) and psPAX2 (plasmid 12260; Addgene), and lentiviral particles were harvested on 2 to 3 days after transfection.

Bone marrow was isolated from B6J.129(Cg)-Gt(ROSA)26Sortm1.1(CAG-cas9*, -EGFP)Fezh/J (Jax 026179) bred to the Vav-Cre +Tet2 fl/fl or control Vav-Cre + background. Following euthanasia, bone marrow was stained with CD117 microbeads (Miltenyl Biotech) and CD117 expressing bone marrow was purified by magnetic column selection. Lin-Sca1+cKit+(LSK) HSPC or CD150+CD48-CD34-CD135-LSK (HSC) antibody cocktail (see supplementary table) was used to stain CD117+ enriched bone marrow. LSK HSPC or HSC were then purified by fluorescence activated cell sorting (FACS) using a Sony MA900 cell sorter. FACS purified HSCs or LSK HSPCs and concentrated viruses were resuspended in PVA based medium²³. Virus generated from HEK293T cells was concentrated via ultracentrifugation for 2 hours at 25000rpm prior to LSK transduction. LSKs were transduced for 30 minutes at 2000rpm by spinfection in presence of polybrene (2µg/ml). After viral transduction, cells were cultured overnight in a humidified incubator at 37 degrees Celsius and subsequently were retro-orbitally injected into lethally irradiated mice (450cGy x2) (10 recipients each per genotype per library).

The transduction of HSPCs or HSCs using our UMI-labeled gRNAs enables identification of descendants of each initial lentiviral transduced cell *in vivo*, as identified by independent unique UMI shared by their progeny. This technology identifies the number of related clones (clone frequency) that survive to the terminal time-point as well as the change in the size (number of cells) of these clones. These measurements can then be related to the genetic perturbation mediated by the corresponding sgRNA. We subsequently pooled the results from all the mice in the *in vivo* screen, within the shared experimental conditions, to maintain adequate coverage of the sgRNA library (97% of the genes were represented across the mouse pool at the terminal analysis). Further details, and discussion of this analysis, is provided in the supplementary methods and in supplementary figure 1.

Competitive Bone Marrow Transplantation

Whole bone marrow cells from Cd45.1/Cd45.2 were mixed with Tet2 fl/fl;Cd45.2 (Tet2 KO), Ncoa4 fl/fl ;Cd45.2 (Ncoa4 KO), or Tet2 fl/fl Ncoa4 fl/fl Cd45.2 (Tet2 KO Ncoa4 KO) in PBS (phosphate buffer saline) at 80:20 ratio. In these mice Cre recombinase expression was driven either by Mx- or Vav- promoter depending on the experiments described. Cells were injected retro-orbitally into lethally irradiated B6.SJL-Cd45.1 recipient mice (450cGy x2). Induction of Cre recombinase expression in the Mx-Cre models was accomplished by intra-peritoneal (i.p.) injection of Poly(I:C) (high molecular weight) (Invivogen) 10mg/Kg, for 3 doses on alternate days in Mx-Cre transgenic mice²⁴.

DFCI IACUC reviewed, authorized and monitors the mouse work used during this study.

Additional methods are enclosed in the supplementary information.

Results

Identification of synthetic lethal vulnerabilities in *Tet2* deficient HSPCs

We generated a library of 12727 single guide RNAs (sgRNAs) targeting 2055 genes (6 sgRNAs per gene) identified as putative epigenetic and transcription factors alongside 354 control sgRNAs. To enable the tracking of the clonal progeny of each cell transduced by a lentivirus, we encoded a nucleotide-based unique molecular identifier (UMI) library within the sgRNA-expressing vector enabling simultaneous clonal tracing of each HSPC transduction event as well as identification of the corresponding CRISPR-Cas9 mediated genetic perturbation (Fig. 1A, Supplementary Fig. 1A), whereby clonally related descendants from the transduced HSPC would share the same UMI-gRNA. The size of the clone could be inferred from the variant allelic frequency (normalized read depth) of the detected UMI-gRNA.

To investigate the genes that are selectively required for clonal fitness in *Tet2* KO compared to WT cells, we transplanted 4 million Cas9-expressing *Tet2* KO or WT Lineage-Sca-1+cKit+ (LSK) HSPCs, which were transduced with our UMI-labeled sgRNA library, into 40 lethally irradiated recipient mice. The screening platform detected each clone with sufficient sequencing depth, maintained adequate representation of library genes during transplantation, and enabled tracking of over 200,000 unique clones with 81-137 cells represented per sgRNA (Supplementary Fig. 1B-F).

We examined bone marrow from mice at 14 weeks post-transplant, a time-point by which transplanted HSCs contribute to the majority of the hematopoietic system¹⁸. We identified 500-2500 unique clones per mouse at this terminal analysis (Supplementary Fig. 1G-H). At this time-point, we quantified the number of surviving clones with sgRNA targeting genes compared to control sgRNAs, as a surrogate for HSC potential. Genes known to cooperate with *Tet2* loss to drive hematological malignancy (e.g. *Bcor* and *Tet3*) resulted in an increase in number of *Tet2* KO clones. (Fig. 1C). *BCOR* loss-of-function mutations have been identified in *TET2*-mutated MDS²⁵, and *Bcor* deletion in *Tet2*-mutant mouse models results in MDS/MPN²⁶. Deletion of *Tet3* has been observed to accelerate the development of *Tet2*-deficient AML in mice²⁷.

We next sought to identify genetic dependencies of *Tet2* KO HSPCs. We hypothesized that sgRNA-mediated gene KOs which result in a reduction in both the number (i.e. unique clones) and size (i.e. variant allelic frequency, related to the number of cells) (Supplemental figure 1A) of *Tet2* KO clones as compared to WT were most likely to represent synthetic lethal vulnerabilities in *Tet2* KO HSPCs (Fig. 1B, Supplementary Fig. 1I, Supplementary Table 2). We identified candidate genes which were associated with a reduction in number of *Tet2* KO clones. Next, we ranked these candidate genes by their effect on *Tet2* KO clone size. Top candidate genes identified by this strategy have recently been shown to contribute to myeloid neoplasia: *Six1*²⁸, *Cdx2*²⁹, *Piwil4*³⁰, *Prmt5*³¹ (Fig. 1D-E, Supplementary Fig. 1I), showing remarkable predictive power to identify genes required for oncogenesis. Our approach identified genetic dependencies in hematological cell lines annotated by the Cancer Dependency Map (DepMap)³² (Supplementary Figure 1J). In contrast, we found that analysis by existing pipelines

(MAGeCK³³) misclassifies known tumor suppressor genes as potential *Tet2* synthetic lethal candidates (Supplementary Table 3)³⁴.

Taken together, we establish the use of a UMI-barcoded CRISPR-Cas9 *in vivo* screen to enable clonal tracing over a long-term transplant, and thereby robustly identify genetic dependencies in *Tet2* KO HSPCs.

***Ncoa4* KO impairs competitive transplantation advantage of *Tet2* KO HSPCs**

To validate the synthetic lethal candidates identified by this screen we used CRISPR-Cas9 to target 24 top candidate genes in CD150+CD48-CD135-LSK HSCs with an independent validation library of sgRNAs. This confirmed that KO of top candidate genes *Cdx2*, *Piwil4*, and *Ncoa4*, resulted in a significant detriment to *Tet2* KO HSC clonal competitiveness (Supplementary Fig. 2A). Having identified and validated putative synthetic lethal targets of *Tet2* mutant HSPCs, we sought to further investigate *Ncoa4*, a top candidate gene, whose role in both normal and *Tet2*-deficient HSPCs was previously unclear. Specifically, we aimed to validate *Ncoa4* as a synthetic lethal target of *Tet2*-mutant HSPCs and understand the underlying impact of *Ncoa4* KO on *Tet2* KO HSPC function. We transduced Cas9-expressing *Tet2* KO or WT HSCs (CD150+CD48-CD135-LSK³⁵) with lentiviral vectors encoding a fluorescent protein in series with *Ncoa4* or control sgRNA (Fig. 2A). This enabled flow cytometry-based tracking of CRISPR-Cas9 modified hematopoietic progeny. This transplantation revealed a progressive reduction in peripheral blood chimerism from *Ncoa4* sgRNA as compared to control sgRNA (Fig. 2B), which was more pronounced in *Tet2* KO than WT.

We next sought to validate the CRISPR-Cas9 screen results by using a transgenic *Ncoa4* KO mouse model³⁶. We first used a Cre recombinase regulated by the Vav promoter; which enabled excision of *Ncoa4* and/or *Tet2* starting from the earliest fetal hematopoietic compartments³⁷ (Fig. 2C). By 12 weeks, the expansion of *Tet2* KO blood cells relative to WT cells was reduced in the setting of *Tet2*; *Ncoa4* double KO (Fig. 2D, Supplementary Fig. 2B). However, there was a reduction in differences in peripheral blood and bone marrow expansion capacity between *Ncoa4* KO; *Tet2* KO and *Tet2* KO in the Vav-Cre driven system at 16 weeks, possibly due to compensatory CD71 upregulation (Figure 2D and Supplementary Figure 2C-D). Despite this compensation, in a secondary transplantation of whole bone marrow, *Tet2*; *Ncoa4* double KO had reduced repopulating capacity compared to *Tet2* KO alone (Fig. 2E, Supplementary figure 2D), demonstrating a long-term functional deficit in *Tet2*; *Ncoa4* double KO as compared to *Tet2* KO HSPCs.

We hypothesized that acute loss of *Ncoa4*, without developmental compensation, would more closely reflect the findings from the CRISPR-Cas9 screen. Therefore, we used a Cre recombinase under the Mx promoter (Mx-Cre), which results in the deletion of *Tet2*, *Ncoa4*, or both following injections of poly(I:C). In a transplantation experiment, bone marrow from WT, *Tet2* KO, *Ncoa4* KO or *Tet2* KO; *Ncoa4* KO was competed against WT in a 20:80 ratio (Fig. 2F). Following excision of *Ncoa4*, *Tet2* KO peripheral blood

chimerism was significantly reduced compared to *Tet2* KO alone in both myeloid and lymphoid fractions (Fig. 2G). Consistent with this observation, this reduction in *Tet2*;*Ncoa4* double KO as compared to *Tet2* KO, was seen in the lineage negative and HSC fractions of the bone marrow (Fig. 2H).

We performed single-cell RNA-sequencing (scRNAseq) on sorted LSK HSPCs containing non-targeting control or *Ncoa4* sgRNAs, to understand the transcriptional effects of *Ncoa4* KO on *Tet2* KO HSPCs. First, we confirmed our observations from the MxCre transgenic, by flow cytometry³⁵, that there was a reduction of HSCs (CD150+CD48-CD135-LSK) expressing *Ncoa4* gRNA compared to control gRNA (Fig. 2I, Supplementary Fig. 2F). Conversely, *Tet2* KO, but not WT myeloid biased multipotent progenitors (MPPs; CD150-CD48+CD135-LSK) increased in number when expressing *Ncoa4* gRNA as compared to control gRNA (Supplementary Fig. 2G). No significant differences in erythroid progenitors were observed in the bone marrow transplantations of WT or *Tet2* KO Cas9 expressing HSCs transduced with *Ncoa4* gRNAs (Supplementary Fig. 2H-I). Cells expressing *Ncoa4* gRNA exhibited lower *Ncoa4* expression, consistent with CRISPR-Cas9 KO (Supplementary Fig. 2J). Pseudo-time analysis positioned HSCs and progenitor cells along the established differentiation trajectory in both WT and *Tet2* KO HSPCs, with and without *Ncoa4* loss^{38,39} (Fig. 2J). Consistent with previously reported HSC markers, *Tcf15*-expressing HSCs resided at the earliest pseudo-time, followed by cells expressing other HSPC markers such as *Cd34*, *Hlf*, *Flt3* and *Kit* (Supplementary Fig. 2K)⁴⁰⁻⁴². HSPCs further along the pseudo-time trajectory expressed surface markers such as *Fcgr3*⁴³, known to be enriched in myeloid progenitors (Supplementary Fig. 2K). Quantification of cells with early pseudo-time signatures revealed that *Ncoa4* loss resulted in a relative decrease in HSCs and a relative increase in progenitor cells, with these effects being more pronounced in *Tet2* KO mice (Supplementary Fig. 2L-M). Similarly, *Ncoa4* loss in *Tet2* KO HSPCs reduced the expression of stem cell gene signatures, to a greater degree than that which is seen in WT HSPCs (Fig. 2K-L, supplementary Fig. 2N). In contrast to these differences in differentiation between *Ncoa4* KO and WT cells, there was no increase in apoptosis following CRISPR-Cas9 mediated KO of *Ncoa4* in WT or *Tet2* KO HSCs (Supplementary Fig. 2O-Q).

In summary, both CRISPR-Cas9 and Cre recombinase-mediated deletion of *Ncoa4* diminished the competitive fitness of *Tet2* mutant hematopoiesis. Acute depletion of *Ncoa4* by CRISPR-Cas9 or a Mx promoter driven Cre recombinase reduces HSC numbers in *Tet2* mutant cells, as observed by flow cytometry and single cell RNA-seq.

Ferritinophagy-dependent labile iron flux is increased in *Tet2* KO HSPCs

Excess intracellular iron is toxic due to increased oxidative stress (e.g. iron-mediated lipid oxidation leading to ferroptosis)⁴⁴; thus, intracellular iron homeostasis is tightly regulated. Excess labile iron (Fe²⁺) is stored in ferritin and is released in response to cellular demands by lysosomal degradation of ferritin⁴⁵, a process known as ferritinophagy. NCOA4 is an adapter for ferritin heavy chain (FTH1), directing FTH1 to autophagosomes resulting in release of labile iron (Fe²⁺) following lysosomal

degradation of their contents^{45,46}. The selective reliance of *Tet2* KO HSPCs on *Ncoa4* suggests that the *Tet2* KO cells have a greater requirement for labile iron. To test this hypothesis, we examined whether iron availability selectively impacts *Tet2* KO cell growth compared to WT cells. To examine this question *in vitro*, we used *Tet2* KO and WT HSPCs immortalized by exogenous expression of a *Hoxb8-ER* fusion⁴⁷. We found that the selective growth advantage of *Tet2* KO *Hoxb8-ER* relative to WT cells was dependent on abundant iron availability in the media (Fig. 3A).

Based on the selective dependency of *Tet2* KO cells on *Ncoa4* and iron availability, we hypothesized that *Tet2* KO cells have increased ferritinophagy to maintain labile iron availability. We assessed ferritinophagy by measuring FTH1 protein levels, including the lysosomal-processed FTH1 product, at steady state and in response to either activators or inhibitors of ferritin degradation (iron chelation or lysosomal protease inhibitors, respectively) (Fig.3B). As expected, the lysosomal cathepsin inhibitor E64D decreased the lysosomal-processed FTH1 product⁴⁶, both at steady-state and after FTH1 degradation stimulated by iron chelation (deferoxamine; DFO) (Fig. 3B, Supplementary Fig. 3A). We found an increase in the lysosome-degraded form of FTH1, consistent with a higher level of ferritinophagy, in *Tet2* KO *Hoxb8-ER* HSPCs compared to WT cells (Fig.3B).

An increase in lysosomal degradation of FTH1 should result in greater labile iron (Fe²⁺) release⁴⁸. To test this, we isolated primary WT and *Tet2* KO HSCs and used an intracellular dye to measure labile iron concentration, with or without DFO treatment to control for the dye specificity. We observed in primary *Tet2* KO HSCs and HSPCs an increase in intracellular labile iron compared to WT, which was dependent on iron chelation (Fig. 3C and Supplementary Fig. 3B). To confirm that intracellular ferritinophagy via *Ncoa4* is a major source of labile iron in *Tet2* KO, we knocked down *Ncoa4* using shRNA, which reduced lysosomal degradation of FTH1 and labile iron pool (Supplementary Fig. 3C-E)⁴⁸. Recovery of HSC expansion and peripheral blood chimerism by week 16 in our VavCre dependent *Ncoa4* KO system, which results in fetal hematopoietic KO of both *Tet2* and *Ncoa4* (Fig. 2C-D)⁴⁹, was associated with an increased expression of the transferrin receptor (CD71⁵⁰) in HSCs and HSPCs (Supplementary Fig. 2C-D). This suggested increased iron uptake followed *Ncoa4* KO to maintain the labile iron demand in *Tet2* KO HSPCs.

Following ferritin degradation, intracellular iron is released from lysosomes. We sought to manipulate labile iron release from lysosomes *in vivo* to investigate whether this mimics the effects of *Ncoa4* KO on *Tet2* mutant hematopoiesis. Lysosomal iron release can be inhibited with ironomycin, which sequesters iron in lysosomes both *in vitro* and *in vivo*⁵¹ (Supplementary Fig. 3F-G). To investigate whether ironomycin has a greater effect on *Tet2* KO HSPCs as compared to WT, we competitively transplanted *Tet2* KO and WT bone marrow at a 20:80 ratio into lethally irradiated recipient mice and monitored engraftment. Following engraftment, recipient mice were treated with a 4-

week intra-peritoneal course of ironomycin (3mg/kg) or vehicle control⁵² (Fig. 3D). Inhibition of lysosomal iron release by ironomycin reduced *Tet2* KO expansion in myeloid but not lymphoid compartments (Fig. 3E, Supplementary Fig. 3H-I), consistent with results from our *Tet2; Ncoa4* double KO VavCre system. *Tet2* KO Lin-Sca1+cKit+ HSPC chimerism decreased in mice treated with ironomycin as compared to control (Fig. 3F).

Taken together, we demonstrate that the increased cell growth of *Tet2* KO relative to WT cells is dependent on iron availability. *Ncoa4* regulates intracellular labile iron, depletion of iron decreases the competitive growth of *Tet2* KO cells, and *Tet2* KO HSPCs have elevated iron levels and increased ferritinophagy compared to WT cells. Pharmacologic inhibition of lysosomal iron release, an alternative mechanism to decrease labile iron availability, phenocopied loss of *Ncoa4*, decreasing the competitive advantage of *Tet2* KO HSPCs.

Ferritinophagy maintains increased mitochondrial ATP production in *Tet2* KO as compared to WT HSPCs

We next sought to identify specific cellular processes that increase iron demand in *Tet2* KO HSPCs compared to WT. We compared scRNA-seq results between WT and *Tet2* KO LSKs transduced with control sgRNA for hematopoietic cells at similar differentiation states in the earliest pseudo-time clusters. Gene set enrichment analysis in *Tet2* KO versus WT HSCs revealed increased expression of oxidative phosphorylation, mitochondrial, and *PGC-1alpha* gene sets (Fig. 4A-B)⁵³.

To complement the analysis of gene sets enriched in *Tet2* KO cells, we performed an *in vivo* genetic screen using our UMI-labelled CRISPR-Cas9 screening platform with a curated library of 4440 sgRNAs targeting 1032 genes related to iron homeostasis and mitochondrial function. The screen highlighted *Steap3*, a ferri-reductase that converts Fe³⁺ to labile Fe²⁺, as one of the top dependencies for *Tet2* KO expansion (Fig. 4C-D, Supplemental Figure 4A). Additionally, genes involved in mitochondrial respiration (*Idh3g*) and mitochondrial translation (*Mief1*) were selectively required for clonal advantage of *Tet2* KO relative to WT cells (Fig. 4C-D). These findings provide further evidence that *Tet2* KO clonal fitness is selectively dependent on labile iron homeostasis and mitochondrial function⁵⁴.

Given the selective dependence of *Tet2* KO HSPCs on mitochondrial synthesis and function, we hypothesized that *Tet2* KO and WT HSPCs might exhibit differences in mitochondrial morphology. Using transmission electron microscopy (TEM), we examined mitochondrial features in WT and *Tet2* KO LSK HSPCs, specifically focusing on mitochondrial cristae morphology. Cristae, the location of the respiratory electron transport chain (ETC), adapt to meet the cell's metabolic demands and these morphological adaptations define cellular respiratory capacity.⁵⁵⁻⁵⁹ Indicative of

increased mitochondrial respiration, *Tet2* KO HSPCs and Hoxb8-ER cells had higher cristae density than that of WT (Fig. 4E-F, Supplementary Fig. 4B). Given that the competitive advantage of *Tet2* KO HSPCs is iron dependent, we investigated whether cristae density in *Tet2* KO Hoxb8-ER cells could be reversed by inhibiting ferritinophagy. Both *Ncoa4* shRNA knockdown and ironomycin treatment reduced the cristae density of *Tet2* KO Hoxb8-ER cells to that of WT cells (Fig.4F, Supplementary Fig. 4B).

To determine if this mitochondrial difference seen in HSPCs extend to HSCs (CD135-CD34-CD48-CD150+LSK), we stained mitochondria in WT and *Tet2* KO HSCs. 3D-Structured-Illumination Microscopy (SIM) images were analysed via a validated pipeline⁶⁰⁻⁶² demonstrating that *Tet2* KO HSCs have increased mitochondrial volume compared to WT (Fig. 4G). Finally, quantitative PCR measurement of mitochondrial DNA suggested increased mitochondrial mass in *Tet2* KO as compared to WT Hoxb8-ER cells (Supplementary Fig. 4C)⁶³.

To assess whether these phenotypic changes corresponded to functional increases in mitochondrial ATP production, we performed mitostress Seahorse assays. Mitochondrial ATP production in *Tet2* KO Hoxb8 HSPCs was markedly increased compared to WT. Once again, this could be reversed with *Ncoa4* knockdown or ironomycin treatment (Fig. 4H, Supplementary Fig. 4D-E). This finding demonstrates that mitochondrial ATP production, in addition to mitochondrial cristae density, is increased in *Tet2* KO cells.

We next sought to determine whether the increase in mitochondrial ATP production observed in *Tet2* KO HSPCs is conserved in human HSPCs. Using human umbilical cord blood CD34+ HSPCs, we edited the genomic loci at either *TET2* or control site (*AAVS1*) using a Cas9-ribonucleotide protein sgRNA complex. To mark CD34+ HSPCs with successful *TET2* editing, an adenovirus vector encoding a fluorescent reporter (mNeonGreen) and a sequence with homology to the edited genomic sites was introduced. This allowed integration of the gene encoding a fluorescent protein at the CRISPR edited site via homologous recombination⁶⁴. We performed mitostress Seahorse assay on the purified, successfully edited control or *TET2* mutated HSPCs. Consistent with the findings in murine cells, human CD34+ cells with an edited *TET2* locus had an elevated mitochondrial ATP production rate (Fig. 4I, Supplementary figure F). Inhibition of ferritinophagy using ironomycin reduced the increase in mitochondrial ATP production seen in *TET2* mutant human CD34+ cord blood cells (Figure 4J).

In summary, in *Tet2* KO HSPCs, we observed increased mitochondria cristae density and mass correlating with a ferritinophagy-dependent increase in mitochondrial ATP production. We note that this ferritinophagy- dependent increase in mitochondrial ATP production was also conserved in human CD34+ HSPCs with *TET2* mutations.

Discussion

We utilized a large-scale barcoded CRISPR/Cas9 screening platform to perform clonally tracked genetic perturbations in HSPCs over long-term transplantation, thereby identifying selective dependencies of *Tet2* KO HSPCs. We identified *Ncoa4* as a vulnerability in our model of *Tet2*-deficient CHIP. NCOA4 is an adaptor protein which directs ferritin to lysosomes, resulting in autophagy-dependent degradation (ferritinophagy). Our data suggests *Tet2* KO HSPCs have increased ferritinophagic flux and an expanded labile iron (Fe²⁺) pool, which is acutely inhibited by *Ncoa4* knockdown. Through microscopy, genetic perturbations, and mitochondrial assays, we demonstrate that *Tet2* deficient HSPCs have increased mitochondrial demand in comparison to WT, and that reducing ferritinophagic flux and labile iron content, either through *Ncoa4* knockdown or ironomycin treatment, reduce mitochondrial ATP production in *Tet2* KO cells.

Utilizing nucleotide-based unique molecular identifiers (UMIs), we were able to track stem and progenitor cells clonally in a large-scale *in vivo* CRISPR/Cas9 KO screen. Our screens demonstrate the capability of this strategy to study stem and progenitor cell biology, which requires long-term tracking of clonal dynamics. For example, by conventional analysis, HSPCs with genetic perturbations against known cancer genetic drivers (e.g. *Dnmt3a*) are mistakenly identified as deleterious to stem-progenitor function because they increase stem cell renewal⁶⁵ and reduce proliferation during hematopoietic differentiation (Supplemental Table 3). The tracking of clonal growth over long-term transplantation using barcodes enables the identification of true genetic dependencies by tracking malignant clones with late clonal growth. Other putative targets requiring further validation may provide novel insights into *Tet2* mutant HSPC biology (Supplemental Table 2). Our ability to identify an important regulator of iron homeostasis as a dependency in HSPCs was contingent on performing this screen *in vivo*, where local iron availability in the HSC niche is dependent on BM macrophages⁶⁶. Prior CRISPR-Cas9 screens in primary HSPCs have been predominantly limited to *in vitro* settings⁶⁷ or to smaller sgRNA libraries⁴⁰. Recent work which is complementary to our approach has utilized an *in vivo* CRISPR-Cas9 screen to assess genetic perturbations and single cell transcriptomics simultaneously (Perturb-seq)⁶⁸. Efforts to understand clonal dynamics using nucleotide barcoded CRISPR-Cas9 screen *in vivo* have been applied to more differentiated cells such as T-cells⁶⁹. The ability to track clonal growth *in vivo* has many potential applications including tracking clonal infiltration into tumors and tissues, and to study normal and malignant cell biology in a physiological setting.

We identified labile iron (Fe²⁺) as a dependency for the competitive advantage of *Tet2* KO HSPCs, which exhibit increased HSC self-renewal⁵ and clonal expansion in CHIP². The importance of iron availability in maintaining HSCs have been recently recognised^{66,70}. *Ncoa4* plays a central role in maintaining this iron dependency by mediating ferritinophagy, the autophagy-dependent degradation of ferritin that releases

Fe²⁺. We confirmed that inhibition of ferritinophagy, either genetically, by *Ncoa4* KO, or pharmacologically, with ironomycin, reduced *Tet2* KO HSC numbers relative to WT HSCs. Our observations that reducing iron availability through *Ncoa4* inhibition reverses the mitochondrial phenotype seen in *Tet2* KO cells is consistent with a prior study in pancreatic cancer showing that *NCOA4* knockdown downregulates mitochondrial iron-sulfur cluster-containing proteins, which are important for the electron transport chain and mitochondrial respiration⁴⁸. The dependency on ferritinophagy observed in *Tet2*-mutant CHIP in our study and in recent work in primary human AML stem cells⁷¹ suggests that ferritinophagy is a dependency across myeloid malignancies. Although iron overload is commonly observed in MDS, *Ncoa4* is overexpressed in bone marrow stem and progenitor cells from MDS patients compared to healthy individuals⁷², highlighting a persistent demand for labile iron and iron chelation appears to improve event-free survival in individuals with MDS⁷³. Agents that inhibit NCOA4 activity are in development for clinical use⁷⁴.

A striking finding of this study is the difference in mitochondrial morphology and function between *Tet2* KO and WT HSPCs. *Tet2* KO HSPCs exhibit increased mitochondrial size and cristae density, compared to WT. Experimental evidence suggests that inhibiting mitochondrial fusion is sufficient to decrease cellular proliferation⁷⁵, indicating a possible link between *Tet2* KO clonal outgrowth and its mitochondrial morphology. Our functional findings are consistent with the observation of increased oxidative phosphorylation gene expression program in HSCs from patients with *TET2* mutated CHIP compared to healthy individuals⁷⁶.

In summary, we identified genetic dependencies of *Tet2* KO stem and progenitor cells using a large UMI-barcoded CRISPR-Cas9 *in vivo* screen. We describe an important role for *Ncoa4*-mediated ferritinophagy, linked to increased iron utilization for mitochondrial ATP metabolism in stem cells, as a mechanism that aids clonal advantage in CHIP and myeloid malignancies.

Acknowledgements:

We are grateful to Vamsi Mootha and Jordan Wengrod for their helpful discussions. J.L. is a recipient of a CRUK-AACR Transatlantic Fellowship. B.L.E. received support for this work from the NIH (R01HL082945, P01CA066996, and R35CA253125), the Howard Hughes Medical Institute, the Edward P. Evans Foundation, and the Adelson Medical Research Foundation. P.G.K. is a recipient of the Burroughs Wellcome Fund Career Awards for Medical Scientists, a Damon Runyon Physician-Scientist supported by the Damon Runyon Cancer Research Foundation (PST-35-21), and received support from the Edward P. Evans Foundation for partial support of this work. C.B.H. received support from NIH T32-CA251062, the Edward P. Evans Foundation, The Academy of

Clinical Laboratory Physicians and Scientists, and the Pan-Mass Challenge FLAMES team. S.A.A. is supported by NIH grant CA066996. Electron Microscopy Imaging, consultation and services were performed in the Harvard Medical School (HMS) Electron Microscopy Facility. Microscopy Resources on the North Quad (MicRoN) core at Harvard Medical School provided 3D imaging.

Authors contributions

J.L., P.G.K., B.L.E. designed the study and wrote the manuscript. J.L., P.G.K., T.T.P.N., M.B., M.M., A.M., W.S., C.B.H., M.E., A.N., P.M.L., performed and analyzed experiments., S.A.A., J.D.M. contributed research tools and helped design the study. All authors reviewed and edited the manuscript.

Conflict of interest:

B.L.E. has received research funding from Novartis and Calico. He has received consulting fees from Abbvie. He is a member of the scientific advisory board and shareholder for Neomorph Inc., Big Sur Bio, Skyhawk Therapeutics, and Exo Therapeutics. C.B.H. has received consulting fees from 48 Bio. S.A.A. has been a consultant and/or shareholder for Neomorph, C4 Therapeutics, Hyku Therapeutics, Stelexis Therapeutics and Nimbus Therapeutics. S.A.A. has received research support from Janssen and Syndax. S.A.A. is an inventor on a patent related to MENIN inhibition WO/2017/132398A1. J.D.M. is an inventor on a patent related to targeting ferritinophagy WO/2015/149006A3. J.D.M. also reports research support from Novartis and Casma Therapeutics and has consulted for Third Rock Ventures and Skyhawk Therapeutics, all unrelated to the submitted work. J.L. has received consulting fees from TScan and Jazz pharmaceuticals. The rest of the authors declare no further conflict of interest.

Reference:

1. Jaiswal S, Fontanillas P, Flannick J, et al. Age-Related Clonal Hematopoiesis Associated with Adverse Outcomes. *New England Journal of Medicine*. 2014;371(26):2488-2498.
2. Fabre MA, de Almeida JG, Fiorillo E, et al. The longitudinal dynamics and natural history of clonal haematopoiesis. *Nature*. 2022;606(7913):335-342.
3. Lee-Six H, Øbro NF, Shepherd MS, et al. Population dynamics of normal human blood inferred from somatic mutations. *Nature*. 2018;561(7724):473-478.
4. Ito S, D'Alessio AC, Taranova OV, Hong K, Sowers LC, Zhang Y. Role of Tet proteins in 5mC to 5hmC conversion, ES-cell self-renewal and inner cell mass specification. *Nature*. 2010;466(7310):1129-1133.

5. Moran-Crusio K, Reavie L, Shih A, et al. Tet2 loss leads to increased hematopoietic stem cell self-renewal and myeloid transformation. *Cancer Cell*. 2011;20(1):11-24.
6. Delhommeau F, Dupont S, Valle VD, et al. Mutation in TET2 in Myeloid Cancers. *New England Journal of Medicine*. 2009;360(22):2289-2301.
7. Comazzetto S, Shen B, Morrison SJ. Niches that regulate stem cells and hematopoiesis in adult bone marrow. *Developmental Cell*. 2021;56(13):1848-1860.
8. Ding L, Morrison SJ. Haematopoietic stem cells and early lymphoid progenitors occupy distinct bone marrow niches. *Nature*. 2013;495(7440):231-235.
9. Decker M, Leslie J, Liu Q, Ding L. Hepatic thrombopoietin is required for bone marrow hematopoietic stem cell maintenance. *Science*. 2018;360(6384):106-110.
10. Mantel CR, O'Leary HA, Chitteti BR, et al. Enhancing Hematopoietic Stem Cell Transplantation Efficacy by Mitigating Oxygen Shock. *Cell*. 2015;161(7):1553-1565.
11. Ramdas B, Mali RS, Palam LR, et al. Driver Mutations in Leukemia Promote Disease Pathogenesis through a Combination of Cell-Autonomous and Niche Modulation. *Stem Cell Reports*. 2020;15(1):95-109.
12. Mistry JJ, Young KA, Colom Díaz PA, Maestre IF, Levine RL, Trowbridge JJ. Mesenchymal Stromal Cell Senescence Induced by Dnmt3a -Mutant Hematopoietic Cells is a Targetable Mechanism Driving Clonal Hematopoiesis and Initiation of Hematologic Malignancy. *bioRxiv*. 2024.
13. McClatchy J, Strogantsev R, Wolfe E, et al. Clonal hematopoiesis related TET2 loss-of-function impedes IL1 β -mediated epigenetic reprogramming in hematopoietic stem and progenitor cells. *Nature Communications*. 2023;14(1):8102.
14. Weinreb C, Rodriguez-Fraticelli A, Camargo FD, Klein AM. Lineage tracing on transcriptional landscapes links state to fate during differentiation. *Science*. 2020;367(6479).
15. Naik SH, Perié L, Swart E, et al. Diverse and heritable lineage imprinting of early haematopoietic progenitors. *Nature*. 2013;496(7444):229-232.
16. Lu R, Neff NF, Quake SR, Weissman IL. Tracking single hematopoietic stem cells in vivo using high-throughput sequencing in conjunction with viral genetic barcoding. *Nature Biotechnology*. 2011;29(10):928-933.
17. Morita Y, Ema H, Nakauchi H. Heterogeneity and hierarchy within the most primitive hematopoietic stem cell compartment. *J Exp Med*. 2010;207(6):1173-1182.
18. Busch K, Klapproth K, Barile M, et al. Fundamental properties of unperturbed haematopoiesis from stem cells in vivo. *Nature*. 2015;518(7540):542-546.
19. Datlinger P, Rendeiro AF, Schmidl C, et al. Pooled CRISPR screening with single-cell transcriptome readout. *Nature Methods*. 2017;14(3):297-301.
20. Griffin GK, Wu J, Iracheta-Vellve A, et al. Epigenetic silencing by SETDB1 suppresses tumour intrinsic immunogenicity. *Nature*. 2021;595(7866):309-314.
21. Kanamori M, Konno H, Osato N, Kawai J, Hayashizaki Y, Suzuki H. A genome-wide and nonredundant mouse transcription factor database. *Biochem Biophys Res Commun*. 2004;322(3):787-793.
22. Meier JA, Zhang F, Sanjana NE. GUIDES: sgRNA design for loss-of-function screens. *Nature Methods*. 2017;14(9):831-832.
23. Wilkinson AC, Ishida R, Kikuchi M, et al. Long-term ex vivo haematopoietic-stem-cell expansion allows nonconditioned transplantation. *Nature*. 2019;571(7763):117-121.

24. Kühn R, Schwenk F, Aguet M, Rajewsky K. Inducible gene targeting in mice. *Science*. 1995;269(5229):1427-1429.
25. Malcovati L, Papaemmanuil E, Ambaglio I, et al. Driver somatic mutations identify distinct disease entities within myeloid neoplasms with myelodysplasia. *Blood*. 2014;124(9):1513-1521.
26. Tara S, Isshiki Y, Nakajima-Takagi Y, et al. Bcor insufficiency promotes initiation and progression of myelodysplastic syndrome. *Blood*. 2018;132(23):2470-2483.
27. Shrestha R, Sakata-Yanagimoto M, Maie K, et al. Molecular pathogenesis of progression to myeloid leukemia from TET-insufficient status. *Blood Adv*. 2020;4(5):845-854.
28. Schmidt CR, Achille NJ, Kuntimaddi A, et al. BCOR Binding to MLL-AF9 Is Essential for Leukemia via Altered EYA1, SIX, and MYC Activity. *Blood Cancer Discovery*. 2020;1(2):162-177.
29. Vu T, Straube J, Porter AH, et al. Hematopoietic stem and progenitor cell-restricted Cdx2 expression induces transformation to myelodysplasia and acute leukemia. *Nature Communications*. 2020;11(1):3021.
30. Bamezai S, Pulikkottil AJ, Yadav T, et al. A noncanonical enzymatic function of PIWIL4 maintains genomic integrity and leukemic growth in AML. *Blood*. 2023;142(1):90-105.
31. Tarighat SS, Santhanam R, Frankhouser D, et al. The dual epigenetic role of PRMT5 in acute myeloid leukemia: gene activation and repression via histone arginine methylation. *Leukemia*. 2016;30(4):789-799.
32. Tsherniak A, Vazquez F, Montgomery PG, et al. Defining a Cancer Dependency Map. *Cell*. 2017;170(3):564-576.e516.
33. Li W, Xu H, Xiao T, et al. MAGeCK enables robust identification of essential genes from genome-scale CRISPR/Cas9 knockout screens. *Genome Biology*. 2014;15(12):554.
34. Zhao M, Kim P, Mitra R, Zhao J, Zhao Z. TSGene 2.0: an updated literature-based knowledgebase for tumor suppressor genes. *Nucleic Acids Res*. 2016;44(D1):D1023-1031.
35. Challen GA, Pietras EM, Wallscheid NC, Signer RAJ. Simplified murine multipotent progenitor isolation scheme: Establishing a consensus approach for multipotent progenitor identification. *Exp Hematol*. 2021;104:55-63.
36. Naiara S-C, Sebastian G, Maria Quiles del R, et al. NCOA4 maintains murine erythropoiesis via cell autonomous and non-autonomous mechanisms. *Haematologica*. 2019;104(7):1342-1354.
37. Georgiades P, Ogilvy S, Duval H, et al. vavCre Transgenic mice: A tool for mutagenesis in hematopoietic and endothelial lineages. *genesis*. 2002;34(4):251-256.
38. Qiu X, Mao Q, Tang Y, et al. Reversed graph embedding resolves complex single-cell trajectories. *Nat Methods*. 2017;14(10):979-982.
39. Cao J, Spielmann M, Qiu X, et al. The single-cell transcriptional landscape of mammalian organogenesis. *Nature*. 2019;566(7745):496-502.
40. Rodriguez-Fraticelli AE, Weinreb C, Wang S-W, et al. Single-cell lineage tracing unveils a role for TCF15 in haematopoiesis. *Nature*. 2020;583(7817):585-589.

41. Sommerkamp P, Romero-Mulero MC, Narr A, et al. Mouse multipotent progenitor 5 cells are located at the interphase between hematopoietic stem and progenitor cells. *Blood*. 2021;137(23):3218-3224.
42. Lehnertz B, Chagraoui J, MacRae T, et al. HLF expression defines the human hematopoietic stem cell state. *Blood*. 2021;138(25):2642-2654.
43. Akashi K, Traver D, Miyamoto T, Weissman IL. A clonogenic common myeloid progenitor that gives rise to all myeloid lineages. *Nature*. 2000;404(6774):193-197.
44. Dixon Scott J, Lemberg Kathryn M, Lamprecht Michael R, et al. Ferroptosis: An Iron-Dependent Form of Nonapoptotic Cell Death. *Cell*. 2012;149(5):1060-1072.
45. Mancias JD, Wang X, Gygi SP, Harper JW, Kimmelman AC. Quantitative proteomics identifies NCOA4 as the cargo receptor mediating ferritinophagy. *Nature*. 2014;509(7498):105-109.
46. Dowdle WE, Nyfeler B, Nagel J, et al. Selective VPS34 inhibitor blocks autophagy and uncovers a role for NCOA4 in ferritin degradation and iron homeostasis in vivo. *Nature Cell Biology*. 2014;16(11):1069-1079.
47. Wang GG, Calvo KR, Pasillas MP, Sykes DB, Häcker H, Kamps MP. Quantitative production of macrophages or neutrophils ex vivo using conditional Hoxb8. *Nature Methods*. 2006;3(4):287-293.
48. Santana-Codina N, Del Rey MQ, Kapner KS, et al. NCOA4-Mediated Ferritinophagy Is a Pancreatic Cancer Dependency via Maintenance of Iron Bioavailability for Iron-Sulfur Cluster Proteins. *Cancer Discov*. 2022;12(9):2180-2197.
49. Perez-Cunningham J, Boyer SW, Landon M, Forsberg EC. Hematopoietic stem cell-specific GFP-expressing transgenic mice generated by genetic excision of a pan-hematopoietic reporter gene. *Experimental Hematology*. 2016;44(8):755-764.e751.
50. Gan T, Jude CD, Zaffuto K, Ernst P. Developmentally induced Mll1 loss reveals defects in postnatal haematopoiesis. *Leukemia*. 2010;24(10):1732-1741.
51. Mai TT, Hamaï A, Hienzsch A, et al. Salinomycin kills cancer stem cells by sequestering iron in lysosomes. *Nature Chemistry*. 2017;9(10):1025-1033.
52. Garciaz S, Guirguis AA, Müller S, et al. Pharmacologic Reduction of Mitochondrial Iron Triggers a Noncanonical BAX/BAK-Dependent Cell Death. *Cancer Discovery*. 2022;12(3):774-791.
53. Mootha VK, Lindgren CM, Eriksson K-F, et al. PGC-1 α -responsive genes involved in oxidative phosphorylation are coordinately downregulated in human diabetes. *Nature Genetics*. 2003;34(3):267-273.
54. Meng F, Fleming BA, Jia X, Rousek AA, Mulvey MA, Ward DM. Lysosomal iron recycling in mouse macrophages is dependent upon both LcytB and Steap3 reductases. *Blood Adv*. 2022;6(6):1692-1707.
55. Nielsen J, Gejl KD, Hey-Mogensen M, et al. Plasticity in mitochondrial cristae density allows metabolic capacity modulation in human skeletal muscle. *J Physiol*. 2017;595(9):2839-2847.
56. Triolo M, Wade S, Baker N, Khacho M. Evaluating mitochondrial length, volume, and cristae ultrastructure in rare mouse adult stem cell populations. *STAR Protocols*. 2023;4(1):102107.
57. Hackenbrock CR. Ultrastructural bases for metabolically linked mechanical activity in mitochondria. I. Reversible ultrastructural changes with change in metabolic steady state in isolated liver mitochondria. *J Cell Biol*. 1966;30(2):269-297.

58. Quintana-Cabrera R, Mehrotra A, Rigoni G, Soriano ME. Who and how in the regulation of mitochondrial cristae shape and function. *Biochem Biophys Res Commun.* 2018;500(1):94-101.
59. Cogliati S, Enriquez JA, Scorrano L. Mitochondrial Cristae: Where Beauty Meets Functionality. *Trends in Biochemical Sciences.* 2016;41(3):261-273.
60. Chaudhry A, Shi R, Luciani DS. A pipeline for multidimensional confocal analysis of mitochondrial morphology, function, and dynamics in pancreatic β -cells. *American Journal of Physiology-Endocrinology and Metabolism.* 2020;318(2):E87-E101.
61. Hemel IMG, Engelen BPH, Lubber N, Gerards M. A hitchhiker's guide to mitochondrial quantification. *Mitochondrion.* 2021;59:216-224.
62. Ball G, Demmerle J, Kaufmann R, Davis I, Dobbie IM, Schermelleh L. SIMcheck: a Toolbox for Successful Super-resolution Structured Illumination Microscopy. *Scientific Reports.* 2015;5(1):15915.
63. Quiros PM, Goyal A, Jha P, Auwerx J. Analysis of mtDNA/nDNA Ratio in Mice. *Curr Protoc Mouse Biol.* 2017;7(1):47-54.
64. Nakauchi Y, Azizi A, Thomas D, et al. The Cell Type-Specific 5hmC Landscape and Dynamics of Healthy Human Hematopoiesis and TET2-Mutant Preleukemia. *Blood Cancer Discovery.* 2022;3(4):346-367.
65. Challen GA, Sun D, Jeong M, et al. Dnmt3a is essential for hematopoietic stem cell differentiation. *Nat Genet.* 2012;44(1):23-31.
66. Zhang D, Gao X, Li H, et al. The microbiota regulates hematopoietic stem cell fate decisions by controlling iron availability in bone marrow. *Cell Stem Cell.* 2022;29(2):232-247.e237.
67. Waarts MR, Mowla S, Boileau M, et al. CRISPR Dependency Screens in Primary Hematopoietic Stem Cells Identify KDM3B as a Genotype Specific Vulnerability in IDH2- and TET2-Mutant Cells. *Cancer Discovery.* 2024.
68. Lara-Astiaso D, Goñi-Salaverri A, Mendieta-Esteban J, et al. In vivo screening characterizes chromatin factor functions during normal and malignant hematopoiesis. *Nature Genetics.* 2023;55(9):1542-1554.
69. Milling LE, Markson SC, Tjokrosurjo Q, et al. Framework for in vivo T cell screens. *J Exp Med.* 2024;221(4).
70. Kao YR, Chen J, Kumari R, et al. An iron rheostat controls hematopoietic stem cell fate. *Cell Stem Cell.* 2024;31(3):378-397.e312.
71. Larrue C, Mouche S, Angelino P, et al. Targeting ferritinophagy impairs quiescent cancer stem cells in acute myeloid leukemia in vitro and in vivo models. *Science Translational Medicine.* 2024;16(757):eadk1731.
72. An W, Feola M, Levy M, et al. Iron chelation improves ineffective erythropoiesis and iron overload in myelodysplastic syndrome mice. *eLife.* 2023;12:e83103.
73. Angelucci E, Li J, Greenberg P, et al. Iron Chelation in Transfusion-Dependent Patients With Low- to Intermediate-1-Risk Myelodysplastic Syndromes. *Annals of Internal Medicine.* 2020;172(8):513-522.
74. Hoelzgen F, Nguyen TTP, Klukin E, et al. Structural basis for the intracellular regulation of ferritin degradation. *Nature Communications.* 2024;15(1):3802.
75. Yao CH, Wang R, Wang Y, Kung CP, Weber JD, Patti GJ. Mitochondrial fusion supports increased oxidative phosphorylation during cell proliferation. *Elife.* 2019;8.

76. Jakobsen NA, Turkalj S, Zeng AGX, et al. Selective advantage of mutant stem cells in human clonal hematopoiesis is associated with attenuated response to inflammation and aging. *Cell Stem Cell*. 2024.
77. Subramanian A, Tamayo P, Mootha VK, et al. Gene set enrichment analysis: A knowledge-based approach for interpreting genome-wide expression profiles. *Proceedings of the National Academy of Sciences*. 2005;102(43):15545-15550.

Figure legends

Figure 1 - A unique molecular identifier barcoded *in vivo* CRISPR-Cas9 screen identifies synthetic lethal targets of *Tet2* knockout driven expansion of hematopoietic stem and progenitor cells

A) Nucleotide encoded unique molecular identifier (UMI) linked to a single guide RNA (sgRNA) expression cassette in a lentiviral vector allows clonal tracing post-transduction. Lentiviral infection of wildtype (WT) or *Tet2* knockout (KO) Cas9 expressing murine Lin-Sca1+cKit⁺ (LSK) hematopoietic stem progenitor cells (HSPCs) were harvested 14 weeks (wk) after transplantation into lethally irradiated (IR) recipients. LTR, long-terminal repeat; BM, bone marrow.

B) Analysis strategy to identify genetic dependencies of *Tet2* KO HSPC growth following UMI-based *in vivo* screening.

C-D) Results of the pooled CRISPR-Cas9 KO screen in *Tet2* KO and WT HSPCs.
C) Candidate genes result in a reduced number of *Tet2* KO clones as compared to WT. P-value was obtained using a Fisher's exact test comparing the number of clones containing non-targeting sgRNAs compared to the number of clones containing gene-specific sgRNAs in WT versus *Tet2* KO.

D) Genes with greater persisting clones in WT (*Tet2* KO – WT clone numbers > 50), were subsequently ranked by *Tet2* KO-specific decrease in clone size (variant allelic frequency; VAF) at 14 weeks and VAF differences were assessed by a Welch's t-test. Row normalized by Z-score. All p-values were adjusted for multiple hypothesis testing via FDR. LSK, Lineage-Sca1+cKit⁺; FDR, false discovery rate.

E) Examination of clone numbers and VAF for the top *Tet2* KO specific target genes identified in the CRISPR-Cas9 screen. Welch's t test: n.s. non-significant, * < 0.01, ** < 0.001, *** < 0.0001.

Figure 2 - *Ncoa4* knockout impair *Tet2* KO competitive advantage in mouse transplant models

A) Competitive transplantation of Cas9 expressing WT or *Tet2* KO hematopoietic stem cells (HSCs) (CD150+CD135-CD48-Lin-Sca1+Kit+) transduced with sgRNA targeting *Ncoa4* (sg*Ncoa4*) or non-targeting control (sgNTG). Lentiviral vector expresses a fluorescent protein, enabling tracing of transduced hematopoietic progeny. IR; irradiated, WT; wildtype, KO; knockout.

B) Serial peripheral blood flow cytometric analysis after transplantation of WT or *Tet2* KO cells containing blue-fluorescent protein (BFP) labelled sgNTG or red-fluorescent protein (RFP) labelled sg*Ncoa4*. Results were normalized to percentage of BFP-labelled cells expressing sgNTG. Significance test by two-way ANOVA. Bars showing mean with SEM (standard error of the mean). N = 9-10 mice per arm.

C) Competition experiment between *Vav-Cre*+;Cd45.1/2 control cells against either *Tet2* fl/fl *Vav-Cre*+;Cd45.2 (*Tet2* KO), *Ncoa4* fl/fl *Vav-Cre*+;Cd45.2 (*Ncoa4* KO), *Tet2* fl/fl *Ncoa4* fl/fl Cd45.2 (*Tet2* KO *Ncoa4* KO) or wild-type (WT) *Vav-Cre*+;Cd45.2 BM cells transplanted at a 80:20 (WT: competitor) ratio, injected into lethally irradiated Cd45.1 recipients.

D) CD45.2 chimerism analysis from peripheral blood at each time point, as a percentage of total donor (CD45.2 and CD45.1/CD45.2) in mice transplanted with *Vav-Cre* transgenic mice as per C). Bars showing mean with SEM. N = 18-20 mice per arm. Unpaired t-test between *Tet2* KO and *Tet2* KO *Ncoa4* KO, * <0.01; **<0.001.

E) Transplant of whole BM from primary *Vav-Cre* transgenic mice (from Figure 2C) into secondary recipients. Peripheral blood analysis of whole BM based on CD45 chimerism. Bars showing mean with SEM. N = 5 mice per arm.

F) Competition experiment between *Mx-Cre*+;Cd45.1/2 control against either *Tet2* fl/fl *Mx-Cre*+;Cd45.2 (*Tet2* KO), *Ncoa4* fl/fl *Mx-Cre*+;Cd45.2 (*Ncoa4* KO), *Tet2* fl/fl *Ncoa4* fl/fl Cd45.2 (*Tet2* KO *Ncoa4* KO) or wild-type (WT) *Mx-Cre*+;Cd45.2 BM cells. BM transplanted at a 80:20 (WT: competitor) ratio into lethally irradiated Cd45.1 recipients. plpC injections 10mg/kg i.p. on alternate days for 3 doses.

G) CD45.2 chimerism analysis from peripheral blood at each time point, as a percentage of total donor (CD45.2 and CD45.1/CD45.2) from F). Bars showing mean with SEM. N = 17-20 mice per arm. Unpaired t-test between *Tet2* fl/fl and *Tet2* fl/fl; *Ncoa4* fl/fl. Dashed line demarcates the start of plpC injections.

H) CD45 chimerism in lineage negative (Lin-), Lin-cKit+ (LK), Lin-Sca1+cKit+ (LSK) and CD150+CD48-LSK (HSC) BM fractions from *Mx-Cre* transgenic mice from 2F) at 11 weeks post-transplant. N=9-10 mice per arm. Unpaired t-test between genotypes indicated.

I) Flow cytometric analysis of HSC and multipotent progenitor (MPP) BM populations from mice transplanted with Cas9-expressing WT or *Tet2* KO HSCs infected with either sgNcoa4 or sgNTG. Results were normalized to percentage of cells expressing sgNTG. Flow gating strategy depicted in Supplementary Figure 2F. Unpaired t-test, bars showing mean with SEM. Each point represents an individual mouse. N = 7-10 mice per arm.

J) Pseudo-time trajectory of WT or *Tet2* KO Cas9 LSK HSPCs transduced with control or *Ncoa4* gRNAs. Analysis was performed using Monocle3. Pseudo-time trajectory annotation with expression of stem and HSPC markers are highlighted in Supplementary Figure 2K.

K) Using cell clusters at the top of the pseudo-time trajectory (blue label), which excludes differentiated Fcgr3+ progenitors, gene set enrichment analysis (GSEA) was performed using all of C2 Molecular Signatures Database⁷⁷. *Tet2* KO HSPCs transduced with control non-targeting gRNAs (gNTG) were compared to *Tet2* KO HSPCs transduced with *Ncoa4* gRNAs (gNcoa4). This revealed enrichment of gene sets expressed in stem cell (red) and leukemia (orange) signatures.

L) Highlighted HSPC gene sets enriched in sgNTG as compared to sgNcoa4 transduced *Tet2* KO HSPCs.

Figure 3 - Expansion of *Tet2* knockout hematopoietic stem and progenitor cells (HSPCs) are dependent on lysosomal dependent ferritinophagy

A) *Tet2* fl/fl; Vav-Cre+ (*Tet2* KO) compared to Vav-Cre+ (WT) Hoxb8-ER immortalized HSPC have increased growth after 4 days in RPMI+10% fetal calf serum (FCS), but not in 1% FCS unless supplemented with ferric ammonium citrate (FAC) (100 μ M). N = 6.

B) Immunoblot of WT and *Tet2* KO Hoxb8-ER HSPC treated with deferoxamine (DFO) 50 μ M, and/or E64D lysosomal protease inhibitor 2 μ g/ml for 16 hours. Immunoblot with ferritin heavy chain (FTH1) and β -Actin antibody. Dashed line: total FTH1 protein, solid line: lysosomal degraded FTH1 product⁴⁶. Fold change quantification of lysosomal degraded FTH1 product, normalized to Beta-Actin and untreated WT cells. N = 3.

C) Cytoplasmic Fe²⁺ pool in HSC from *Tet2* KO as compared to WT. Median fluorescent intensity of labile iron stain relative to untreated WT. Cells either treated with DFO at 50 μ M or vehicle control during concurrent staining, to demonstrate specificity of labile iron stain. Each dot represents an individual mouse. Gating strategy as per Supplementary Figure 2F. Representative flow cytometry histogram of HSCs from WT or *Tet2* KO mice. N = 7.

D) Schematic of a competition experiment between WT or *Tet2* KO CD45.2+ (20% composition) vs. WT CD45.1+/CD45.2+ control (80% composition) BM cells transplanted into lethally irradiated (IR) CD45.1 recipients. Following engraftment at 4

weeks (wk), mice were treated with 4-week treatment of ironomycin (3mg/kg i.p. 5 days per week) vs vehicle prior to harvest for peripheral blood and BM.

E-F)

E) Peripheral blood analysis of whole blood and CD11b compartments and F) BM analysis of CD45.2+ *Tet2* KO and CD45.1+/CD45.2+ WT donor chimerism following 4-week treatment of either ironomycin or vehicle control. Each point represents an individual mouse. N=12-15 per arm.

Bars show mean with SEM, with unpaired t-test used unless otherwise specified.

Figure 4 - Increased Mitochondrial ATP production in *Tet2* KO HSPCs is dependent on ferritinophagy

A) Using cell clusters at the top of the pseudo-time trajectory (blue label) (from Figure 2J), which excludes *Fcgr3*+ differentiated progenitors, GSEA was performed comparing WT vs *Tet2* KO HSPCs using all of C2 Molecular Signatures Database. (Subramanian, Tamayo, et al. PNAS 2005). This revealed enrichment of gene sets involved in mitochondrial function (green) and oxidative phosphorylation (purple).

B) Highlighted mitochondrial and oxidative phosphorylation gene sets comparing WT vs *Tet2* KO HSPCs.

C) Targeted CRISPR screen using mitochondrial and iron homeostasis regulatory genes in WT and *Tet2* KO Cas9 LSK HSPCs. *Tet2* KO HSPCs exhibit genetic dependency to regulators of iron, mitochondrial respiration, and translation. Highlighted genes have false-discovery rate (FDR) < 0.25, WT / *Tet2* KO persisting clone differences > 2, and WT / *Tet2* KO VAF > 1.

D) Doxycycline inducible Cas9 expressing WT or *Tet2* fl/fl *Vav1*-Cre (*Tet2* KO) in *Hoxb8* HSPC system transduced with either control sgRNA (NTG), or C) *Steap3* targeting sgRNA (sg1 and sg2) or *Idh3g* targeting sgRNA (sg1 and sg2). Growth relative to no doxycycline treated cells at 4 days. N=5. Bars showing mean±SEM, unpaired t-test.

E) Transmission electron microscopy (TEM) of primary WT and *Tet2* KO Lin-*Sca1*+*cKit*+ (LSK) HSPCs. Cristae number normalized to length of mitochondria. Scale bar = 500nm. N=50-57 mitochondria from 5 mice per genotype. Mean and SEM displayed with results of unpaired t-test.

F) TEM of WT and *Tet2* KO *Hoxb8* with either control shRNA, *Ncoa4* shRNA or Ironomycin treatment 50nM for 48hrs. Images in Supplementary Fig 4A. Cristae number was normalized to the length of mitochondria. N=30-71 mitochondria per experimental condition. Mean and SEM displayed with results of unpaired t-test.

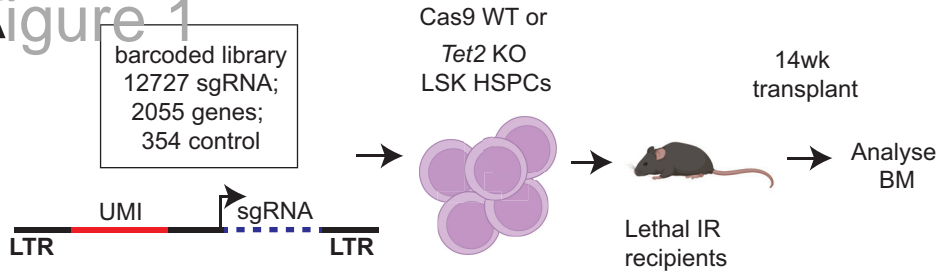
G). Mitochondrial staining of primary WT and *Tet2* KO CD135-CD48-CD34-CD150+ hematopoietic stem cells (HSCs). Scale bar = 5 μ M. Representative slice from 3D-Structured-Illumination Microscopy (SIM) image shown. Quantification of mean volume divided by counted mitochondria. Bars showing mean \pm -SEM, with unpaired t-test. Each dot represents analysis of individual cell from 5 mice per genotype.

H). Representative Mitostress Seahorse assay of WT and *Tet2* KO Hoxb8 treated with either vehicle (DMSO) or ironomycin (50nM) for 48hrs. Oligo: oligomycin, AMA/Rot: Antimycin A/Rotenone, FCCP: Carbonyl cyanide-p-trifluoromethoxyphenylhydrazone. Quantification of mitochondrial and glycolytic ATP production shown in Supplementary Fig 4.

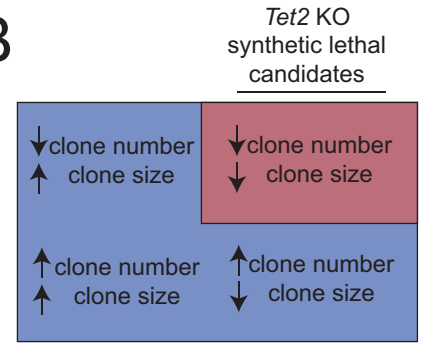
I) Primary human CD34+ umbilical cord HSPCs were transfected with either *AAVS1* or *TET2* (sg1 and sg2) gRNA- CRISPR-Cas9 ribonucleoprotein (RNP) complexes. Adenovirus encoding mNeon-green sequence with adjoining DNA sequence homologous to edited loci, results in integration at targeted genes. After sorting successfully edited cells via fluorescent expression, cells were analyzed with Mitostress Seahorse assay. Mitochondrial ATP production rate derived from oxygen consumption rate (OCR) and extracellular acidification rate (ECAR). N=7. KI, knock-in.

J) Primary human CD34 HSPCs transfected with either *AAVS1* or *TET2* targeting gRNA were treated with either DMSO (Vehicle) or Ironomycin 200nM for 48hrs. N=2-6. Mean, SEM displayed with results of unpaired t-test.

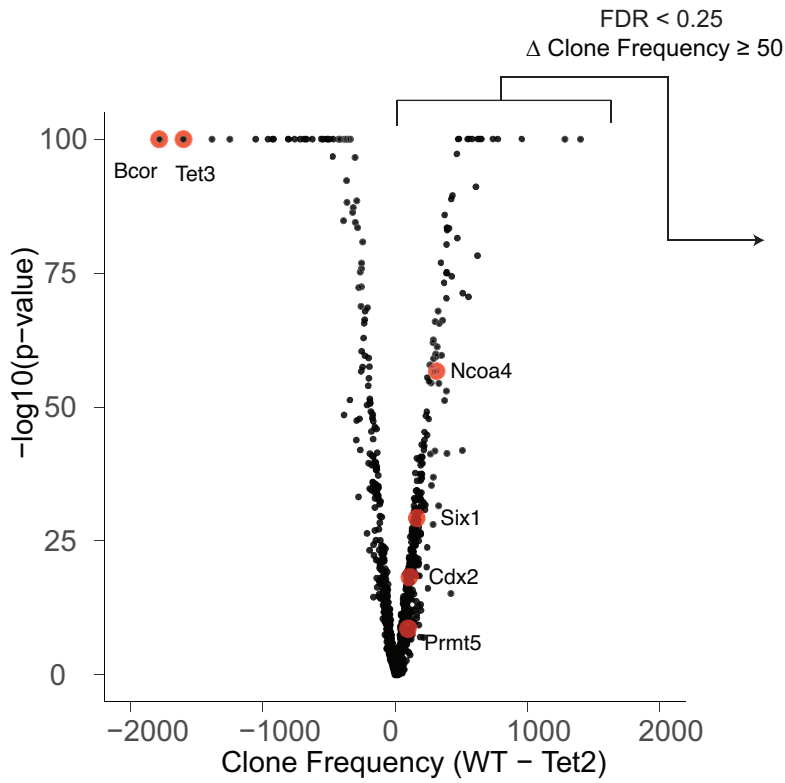
Figure 1



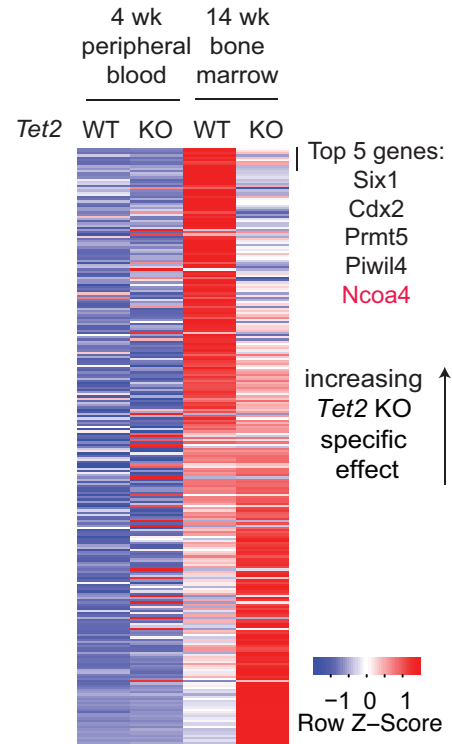
B



C



D



E

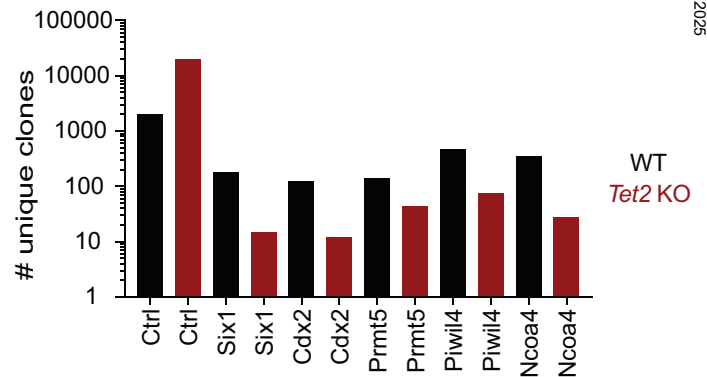
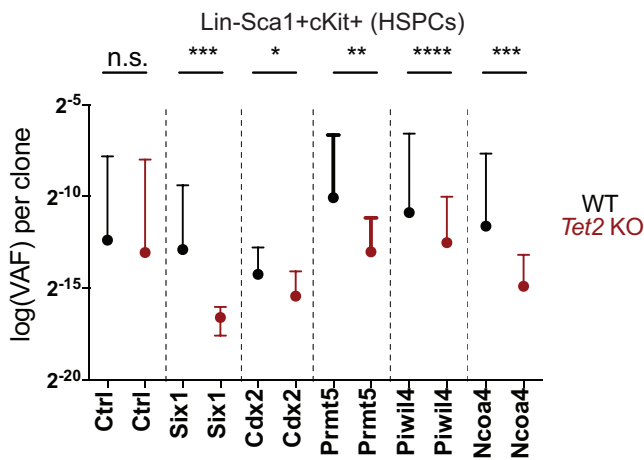


Figure 2

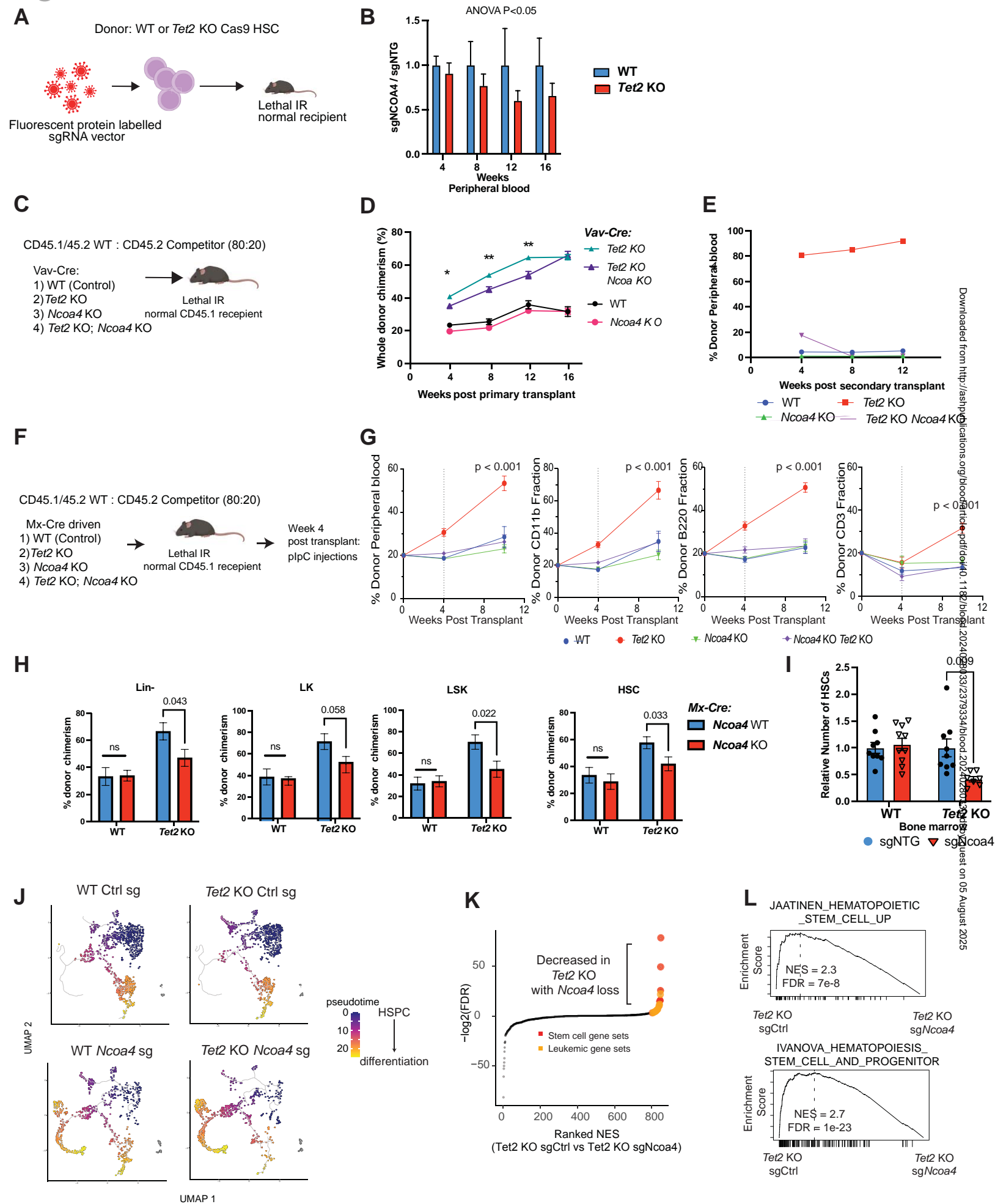


Figure 3

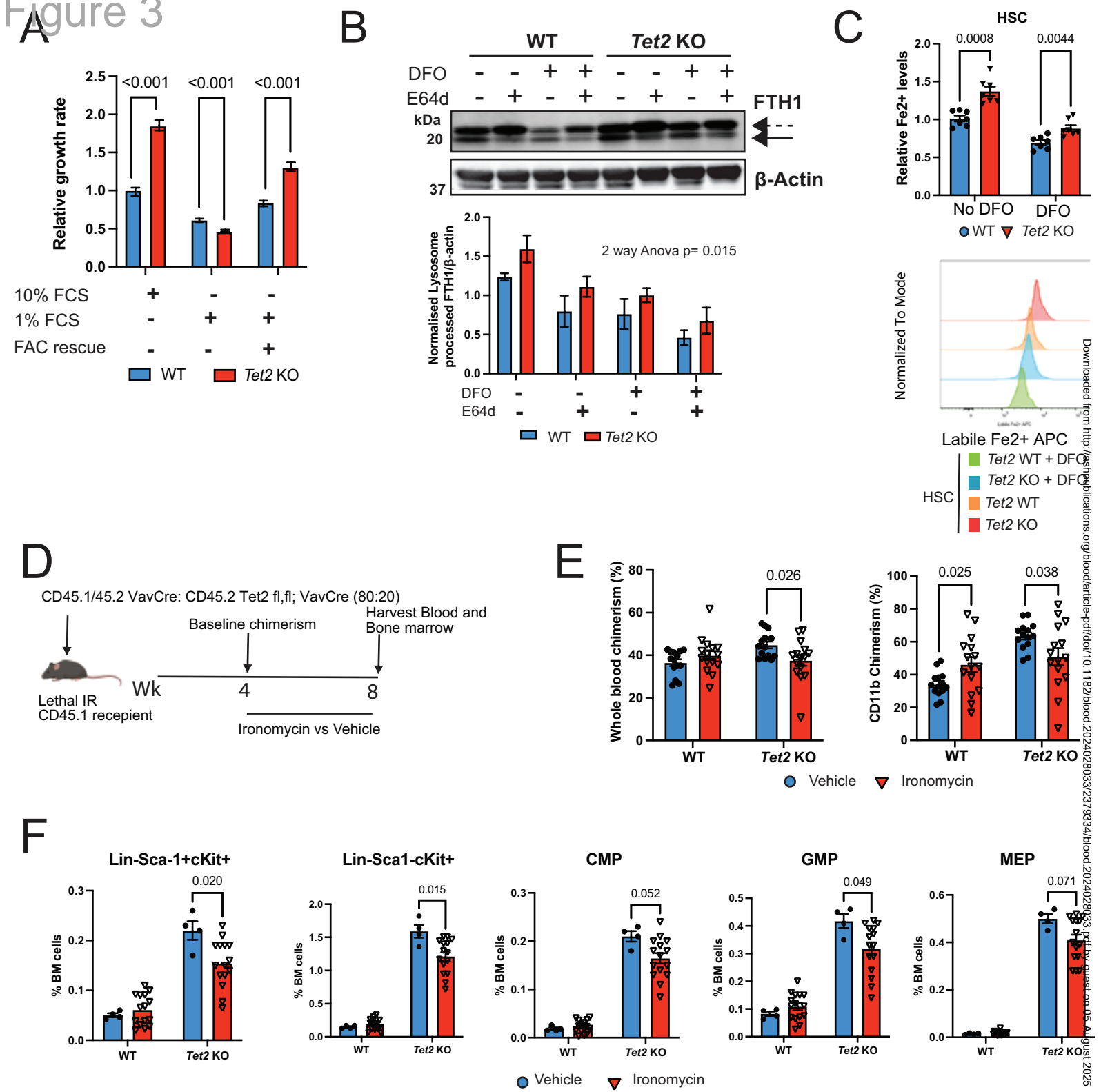
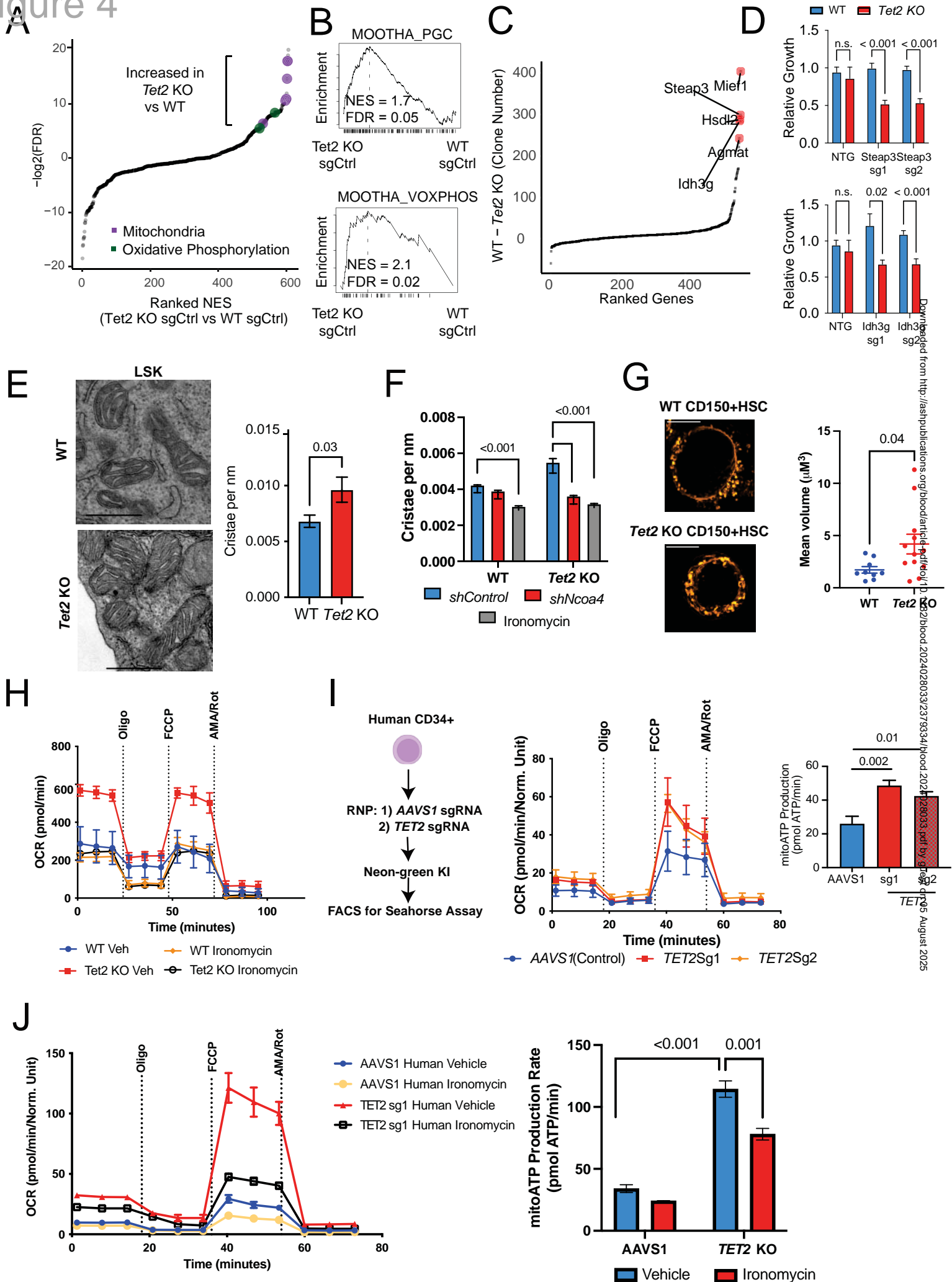


Figure 4



Downloaded from <http://ashpublications.org/blood/article/135/10/2024028033/2379334> by guest on August 20, 2025

Identification of genetic dependencies in *Tet2* KO hematopoietic stem progenitor cells (HSPC)

Context of Research

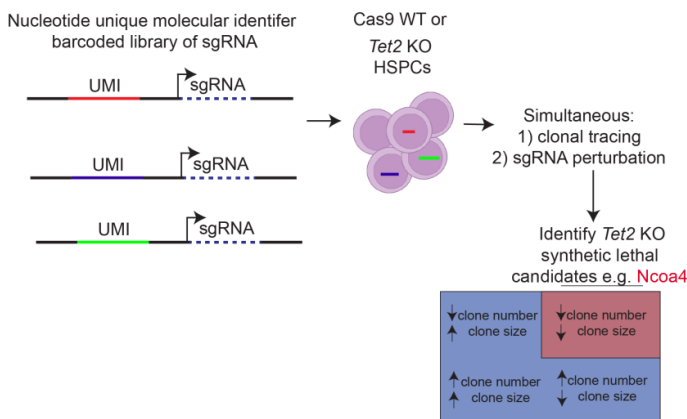
Genetic screens can identify selective dependencies in somatically mutated cells. *Tet2* knockout (KO) expand more rapidly than wildtype hematopoietic stem and progenitor cell (HSPC).

Aim of This Study

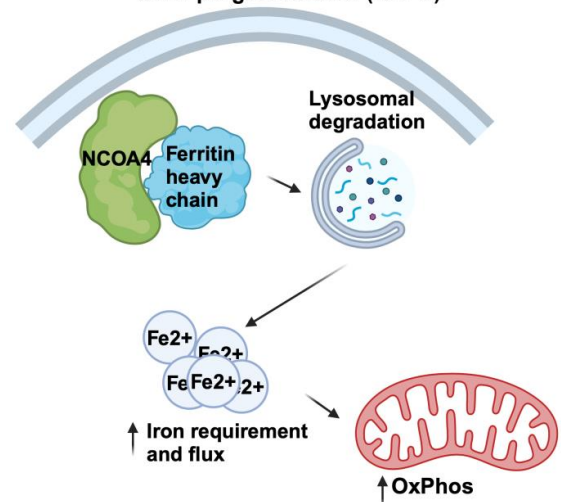
To develop a CRISPR-Cas9 screening method for *in vivo* application, in order to identify regulators of *Tet2* KO HSPC expansion.

Findings

Identification of genetic dependencies in *Tet2* KO hematopoietic stem progenitor cells (HSPC)



Role of ferritinophagy in *Tet2* KO hematopoietic stem progenitor cells (HSPC)



Conclusions:

- 1) Barcoded *in vivo* CRISPR-Cas9 knockout screen identify *Ncoa4* as a dependency in *Tet2* mutant hematopoietic stem-progenitor cells.
- 2) In *Tet2* mutant stem-progenitor cells, *Ncoa4*-mediated ferritinophagy maintains iron availability for increased mitochondrial ATP production.

Loke, Kim et al. DOI: 10.xxxx/*blood*.2024xxxxxx